VARIATION IN CRYPT SIZE AND ITS INFLUENCE ON THE ANALYSIS OF EPITHELIAL CELL PROLIFERATION IN THE INTESTINAL CRYPT

JOHN TOTAFURNO, MATTHEW BJERKNES, AND HAZEL CHENG
Department of Anatomy, Medical Sciences Building, University of Toronto, Toronto, Ontario, Canada M5S 1A8

ABSTRACT The standard model of epithelial cell renewal in the intestine proposes a gradual transition between the region of the crypt containing actively proliferating cells and that containing solely terminally differentiating cells (Cairnie, Lamerton and Steel, 1965*a*, *b*). The experimental justification for this conclusion was the gradual decrease towards the crypt top of the measured labeling and mitotic indices. Recently, however, we have proposed that intestinal crypts normally undergo a replicative cycle so that at any time in any region of the intestine, crypts will be found to have a wide range of sizes. We show here that if this intrinsic size variation is taken into account, then a sharp transition between the proliferative and nonproliferative compartments of individual intestinal crypts is consistent with the labeling and mitotic index distributions of mouse and rat jejunal crypts. Thus there is no need to invoke the region of gradual transition from proliferating to nonproliferating cells as is done in the standard model. The position of this sharp transition is estimated for both the mouse and rat. Experiments to further test our model are suggested and the significance of the results discussed.

I. INTRODUCTION

The standard model of cell proliferation in the epithelium of intestinal crypts is currently the slow cut-off model of Cairnie et al. (1965*a*, *b*) in which a gradual transition from proliferating to nonproliferating cells occurs over a wide range of cell positions within the crypt. In their study of rat intestinal crypts, Cairnie et al. rejected a sharp spatial transition (their sharp cut-off model) between the proliferative and nonproliferative states because of the apparently slow decrease up the crypt that they observed in the mitotic index.

Implicit in the line of reasoning leading to the rejection of the sharp cut-off model is the assumption that the experimentally determined labeling and mitotic index distributions are representative of the kinetics of individual crypts even though they are obtained by averaging over many crypts. From this point of view, any inhomogeneity in the crypt population is attributable to biological noise. The measurement process is assumed to average over such noise, producing distributions that correspond to those of some idealized average crypt. Recently, however, we have attempted to demonstrate that inhomogeneity in the crypt population has a dynamic basis in the cycling of crypts (Totafurno et al., 1987). We have argued that individual crypts in the adult cycle through stages of growth and division. This leads to a population of crypts with widely varying sizes. Such intrinsic nonrandom variation in the crypt population suggests that the population averaged distributions which are usually obtained are not equivalent to those that apply to individual crypts.

Suppose that the mitotic index at a given cell position varies with crypt size. Averaging over the crypt population could then itself be the reason that the population averaged mitotic index distribution decreases more gradually than expected on the basis of the sharp cut-off model alone.[1] Although Cairnie et al. (1965*a*) are careful to record the variation in crypt length, they do not incorporate its effects explicitly into their model. Later authors (Cairnie and Bentley, 1967; Wright et al., 1972) have dealt with the size variation by introducing an ad hoc normalizing scheme in their data collection. Here we derive a quantitative model of the population averaged distributions that assumes the validity of the sharp cut-off model as applied to individual crypts but permits the cell position of the cut-off to vary with crypt size. The model's predictions for both the mouse and rat are found to be consistent with the data. As a result

Address all correspondence to Matthew Bjerknes.

[1]To illustrate, imagine crypts came in only three sizes: 20, 30, and 40 cell positions tall, respectively. Now consider the mitotic index at cell position 20. For the shortest crypts the mitotic index at cell position 20 would be expected to be 0%; in the mid-sized crypts it might be ~3%; and in the tallest crypts the mitotic index in position 20 might be perhaps 5%. Let us suppose further that 50% of crypts are small, 30% are mid-sized, and the remaining 20% are tall. Then a random sampling of cells from position 20 would produce an average mitotic index with the intermediate value of $([0.5][0] + [0.3][0.03] + [0.2][0.05]) \times 100 = 1.9\%$.

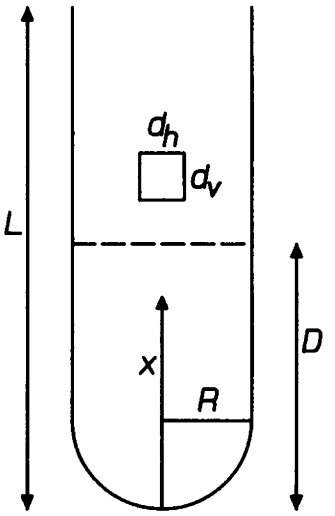

FIGURE 1 Schematic representation of an idealized crypt of length L with a hemispherical base of radius R. The x coordinate is shown with origin at the bottom of the crypt. The dashed line indicates the location of the cut-off at a distance $x = D$ above the bottom of the crypt. The definitions of the widths d_h and d_v are illustrated by the rectangle representing the basal projection of a crypt cell from the cylindrical portion of the crypt.

we conclude that a relatively sharp transition between proliferating and nonproliferating cells in the crypt remains a tenable alternative to the gradual transition proposed by the standard model.

II. The Model[2]

(a) Index Distributions. The labeling index, mitotic index, and growth fraction are measures of cell proliferation which vary both within the crypt and, as we have suggested in the Introduction, between crypts. For convenience we refer to the distributions of these measures within the crypt collectively as index distributions. The index distributions are taken to be continuous functions of the distance along the crypt axis measured from the bottom of the crypt. When this distance is expressed in terms of some physical length unit such as microns (μm), we denote it by x (see Fig. 1). Alternatively, this distance is denoted by p when it is expressed in terms of number of cell positions. As used here, p is effectively a measure of arc length along the crypt perimeter. Because of the hemispherical shape of the crypt base, the transformation between x and p (see Section II[e]) does not correspond simply to a change in units thus necessitating for clarity the use of distinct symbols. Unless explicitly indicated, variables representing lengths in the model will refer to quantities measured in some physical length unit.

Variation between crypts of the index distributions will be assumed for simplicity to depend only upon crypt size and in particular crypt volume, v. Thus we assume that a given position x (or p) is equivalent as regards the index distributions in all crypts with the same volume v. Because average cell volume probably does not vary much between crypts and because crypt length scales as $v^{1/3}$ (see below), crypt volume should be roughly interchangeable in characterizing crypt size with the number of cells in the crypt or with crypt length. We conclude then that the labeling index, mitotic index and growth fraction are functions both of x (or p) and v and denote them by $\lambda(x; v)$, $\mu(x; v)$, and $\gamma(x; v)$, respectively. For convenience, the function $\Phi(x; v)$ is used to refer collectively to the index distributions.

The functions $\Phi(x; v)$ or $\Phi(p; v)$ describe the index distributions of individual crypts. As discussed in the Introduction, these index distributions must be distinguished from the experimentally measured curves which correspond to averages over all of the different sized crypts in the crypt population. We represent the population averages of these distribution by $\langle\Phi\rangle(x)$ or $\langle\Phi\rangle(p)$.

(b) Crypt Population Averaging. The population averaged index distribution $\langle\Phi\rangle(p)$ (or $\langle\Phi\rangle(x)$) is obtained from $\Phi(p; v)$ (or $\Phi(x; v)$) by averaging over the ensemble of crypt volumes. If $f(v)$ is the probability density of a crypt having volume v, then

$$\langle\Phi\rangle(p) = \int_{V_0}^{V_0+\Delta V} \Phi(p; v) f(v)\, dv, \tag{1}$$

where crypt volumes range from V_0 to $V_0 + \Delta V$. As defined here, $\langle\Phi\rangle(p)$ is the expected number of labeled, mitotic or cycling cells at position p divided by the total number of crypts sampled (see Section V[b]). The form of $f(v)$ has been shown to be (Totafurno et al., 1987)

$$f(v) = \frac{2 \ln 2}{\Delta V} \exp\left[-\frac{\ln 2}{\Delta V}(v - V)\right] \tag{2}$$

($V_0 \le v \le V_0 + \Delta V$), with expected value

$$\bar{v} = V_0 + \Delta V\left(\frac{1}{\ln 2} - 1\right). \tag{3}$$

(c) Sharp Cut-off Model. The sharp cut-off model of Cairnie et al. (1965*b*) is assumed to describe the kinetics of individual crypts of volume v. In this model, there is a point along the crypt, $x = D$, above which only nonproliferating cells are produced as proliferating cells migrate past D and complete their last cell cycle. Our derivation of the index distributions follows that of Cairnie et al. (1965*b*) which should be consulted for a fuller justification of the steps involved. Unlike their work, however, parameters such as the sharp cut-off, D, are understood to be dependent on crypt volume and the top of the proliferative zone is no longer assumed to be necessarily at the position $x = 2D$.

The crypt is assumed to be in an approximate steady state (crypt growth is slow; see Totafurno et al., 1987) with cells at a given cell position migrating to positions higher in the crypt at a velocity prescribed by the cumulative cell production below that cell position. Let the phase of a cell in the cell cycle be denoted by $\sigma = t/T$, where t is the age of

[2]For convenience, the symbols used here together with a brief definition are listed in Appendix A.

the cell and T is the cell cycle time which, for simplicity, is assumed uniform throughout the crypt. Thus $0 \le \sigma \le 1$. At cell positions just below the cut-off point, $D(v)$, the distribution of cycling cells through the cell cycle is taken to be that of an expanding population with growth fraction γ_0. The probability of a cell at D being a cycling cell with phase σ is therefore given by

$$P(\sigma)\, d\sigma = 2\gamma_0 \ln 2 \exp(-\sigma \ln 2)\, d\sigma. \quad (4)$$

As the cells at the cut-off D move to higher positions in the crypt, additional noncycling cells are produced. It is assumed that at positions between the cut-off and the top of the proliferative zone, the phase distribution $P(\sigma)$ of these additional noncycling cells (each of which has an age less than or equal to T) and the remaining cycling cells is still given by Eq. (4) with σ for these noncycling cells being interpreted as their age divided by T (see Cairnie et al., 1965*b*). Let the top of the proliferative zone be at position $x = \rho D$. The cycling cells at a position x between D and ρD have phases $\sigma \ge \sigma_{min}(x)$ where $\sigma_{min}(x)$ is the minimum phase of the cycling cells at x and equals the time t it takes for cells at D to migrate to position x divided by the cell cycle time T. To obtain σ_{min} as a function of x, we assume for convenience, as did Cairnie et al. (1965*b*), that cell velocity is roughly proportional to x.[3] Then

$$x = D(v) \exp\left(\frac{t}{T} \ln \rho\right) = D(v) \exp(\sigma_{min} \ln \rho), \quad (5)$$

where $\rho(v)$ is defined so that $x = \rho D$ is the top of the proliferation zone.

The growth fraction just below $D(v)$ is assumed uniform and of value γ_0. Between D and ρD, the growth fraction decreases as cycling cells complete their last cell cycle (see above). The proportion of cells still cycling at a positon x in this region is given by the area under the phase distribution curve between $\sigma = \sigma_{min}$ and $\sigma = 1$ so that

$$\gamma(x) = \int_{\sigma_{min}}^{1} P(\sigma)\, d\sigma. \quad (6)$$

With increasing x, the growth fraction γ decreases until it reaches 0 at the top of the proliferation zone. Thus the growth fraction distribution can be seen as having three regions: a region below the cut-off $D(v)$ where the growth fraction is γ_0; a region between $D(v)$ and $\rho D(v)$ where the growth fraction decreases as given by Eq. (6); and a region above $\rho D(v)$ where the growth fraction is 0 (see Eq. (7) below).

The labeling and mitotic index distributions also have three regions. At positions near $D(v)$ the labeling and mitotic indices have their maximum value which we denote by λ_0 and μ_0, respectively. At positions near $\rho D(v)$, these distributions have the value 0. The intermediate regions (throughout which $\lambda(x)$ and $\mu(x)$ are decreasing) begin at a position x where the phase of the youngest cycling cells σ_{min} corresponds to the beginning of S phase or the beginning of the mitotic phase of the cell cycle, respectively, and end where σ_{min} corresponds to the end of S phase or the end of the mitotic phase (i.e., $\sigma_{min} = 1$), respectively. Within these regions, $\lambda(x)$ and $\mu(x)$ are given by Eq. (6) with the limits of integration changed accordingly. To obtain the labeling index, mitotic index and growth fraction distributions as functions of x, the equations for these distributions (cf., Eq. [6]) were evaluated with the help of Eq. (5). Defining T_s to be the duration of the S-phase of the

[3]This approximation gives a cell velocity at any given x in $D \le x \le \rho D$ that is only slightly greater, for the range of parameters of interest here (i.e., $\rho \sim 2$, $\gamma_0 \sim 1$), than that expected on the basis of our assumption of a steady state.

We may derive the dependence of cell velocity on x from the steady state assumption as follows. Consider the cylindrical portion of a crypt. Let us assume that all cells at a given position x move up the crypt with the same average speed $s(x)$. Also let $n(x)$ be the number density of cells at x. By the steady state assumption, both $s(x)$ and $n(x)$ have no explicit time dependence. The rate at which cells move past a point x is given by $n(x)s(x)$. If the crypt is in a steady state, we have the balance equation (assuming that cell death is negligible in the cylindrical portion of the crypt)

$$n(x)s(x) = n(x_0)s(x_0) + \int_{x_0}^{x} G(y)dy,$$

where x_0 and x ($x_0 < x$) are points in the cylindrical part of the crypt, and $G(x)$ is the rate of cell production at x. In the cylindrical portion of the crypt, the number of cells per unit length, n, is independent of x. Differentiating the balance equation with respect to x therefore gives

$$\frac{ds(x)}{dx} = \frac{1}{n} G(x).$$

Between D and ρD, the rate of cell production, $G(x)$, as implied by Eq. (4) is also independent of x and equal to $(\gamma_0 n \ln 2)/T$ so that

$$\frac{ds(x)}{dx} = \frac{\gamma_0 \ln 2}{T},$$

where $D \le x \le \rho D$. By solving this equation we therefore find that cell velocity is related to x as

$$s(x) = \frac{\gamma_0 \ln 2}{T}(x - D) + s_D,$$

where s_D is the cell velocity at D.

Consider now the position x of a single cell as it moves up the crypt. The speed of this cell, dx/dt, equals $s(x)$. Therefore

$$\frac{dx}{dt} = \frac{\gamma_0 \ln 2}{T}(x - D) + s_D.$$

If we solve this equation subject to the constraints that at $t = 0$, $x = D$, and at $t = T$, $x = \rho D$, then t/T can be identified as σ_{min} and the solution is

$$x(\sigma_{min}) = \frac{(\rho - 1)D}{(e^{\gamma_0 \ln 2} - 1)} e^{\gamma_0 \ln 2 \sigma_{min}} + \frac{D(e^{\gamma_0 \ln 2} - \rho)}{(e^{\gamma_0 \ln 2} - 1)}.$$

When $\gamma_0 = 1$ and $\rho = 2$, which as it turns out are the values we have used (see Section IV [*a*]), this equation for $x(\sigma_{min})$ is identical to Eq. (5).

cell cycle, we find that the index distributions of a crypt of volume v are given by

$$\Phi(x; v) = \begin{cases} A, & \frac{x}{D} \le \alpha_x \\ 2\gamma_0(D/x)^{\ln 2/\ln \rho} - B, & \alpha_x \le \frac{x}{D} \le \beta_x \\ 0, & \frac{x}{D} \ge \beta_x, \end{cases} \quad (7)$$

where A, B, α_x, and β_x are as listed in Table I and D is a function of volume. Here, $D\alpha_x$ and $D\beta_x$ correspond to the points x between D and ρD at which $\sigma_{\min}$ equals the initial and final phases σ, respectively, relevant to the given index distribution (e.g., the phase at the beginning and end, respectively, of S). For given T_s/T, λ_0 must have a value in the range

$$\gamma_0\left[\exp\left(\frac{T_s}{T}\ln 2\right) - 1\right] \le \lambda_0 \le 2\gamma_0\left[1 - \exp\left(-\frac{T_s}{T}\ln 2\right)\right] \quad (8)$$

depending upon the duration of the G_1 phase.

(d) Volume Dependence of Crypt Parameters. We assume for simplicity that the linear dimensions of the crypt, the height of the cut-off (D) and the height of the top of the proliferative zone (ρD) increase uniformly with crypt size. Thus crypt length L is related to volume v by the relation

$$L = av^{1/3}, \quad (9)$$

where a is a measured constant. It also follows that

$$D(v) = D_0\left(\frac{v}{V_0}\right)^{1/3} = D_0\left(\frac{L}{L_0}\right), \quad (10)$$

where D_0, V_0, and L_0 are the cut-off height, volume and length, respectively, of the smallest crypts in the population. A direct check of Eq. (9) reported later in the paper shows that it is consistent with measurements of crypt length and volume. Furthermore, the assumption that ρD increases uniformly with crypt size is consistent with the nature of the growth of the proliferative compartment after 30% resection in the mouse (Bjerknes and Cheng, 1981*b*, p. 94).

TABLE I
DEFINITION OF QUANTITIES IN THE EXPRESSION FOR THE THREE SHARP CUT-OFF INDEX DISTRIBUTIONS*

	λ	μ	γ
A	λ_0	μ_0	γ_0
B	$\lambda_0\left[\exp\left(\frac{T_s}{T}\ln 2\right) - 1\right]^{-1}$	γ_0	γ_0
α_x	$\left\{\frac{2\gamma_0}{\lambda_0}\left[1 - \exp\left(-\frac{T_s}{T}\ln 2\right)\right]\right\}^{\frac{\ln\rho}{\ln 2}}$	$\rho\left(\frac{\mu_0}{\gamma_0} + 1\right)^{-\frac{\ln\rho}{\ln 2}}$	1
β_x	$\exp\left(\frac{T_s}{T}\ln\rho\right)\alpha_x$	ρ	ρ

*See Eq. (7); for definition of parameters see Section II.

As a convenient measure of crypt size variation, we introduce

$$\theta = \frac{L_{\max}}{L_0} = \left(\frac{V_0 + \Delta V}{V_0}\right)^{1/3}, \quad (11)$$

where $L_{\max}$ is the maximum length of crypts in the population and ΔV is the range of crypt volumes in the population. From Eq. (10) we see that D ranges (depending upon the size of the crypt) from D_0 to

$$D_{\max} = \theta D_0. \quad (12)$$

Since both $\rho D(v)$ and $D(v)$ are assumed proportional to $v^{1/3}$, ρ is a constant independent of crypt volume. ρ is such that the number of cells between $D(v)$ and $\rho D(v)$ equals the number of cycling cells below $D(v)$. This may be seen as follows.

Given steady state, the number of cells that move up past D in one cell cycle time equals the number of cycling cells below D. Over the same cell cycle time, all of the cells between D and ρD move out of this region given that all cells above D move consistently towards the crypt top. Thus for steady state to hold, the number of cells between D and ρD must equal the number of cycling cells below D (cell loss over one cell cycle time is negligible for our purposes [Bjerknes and Cheng, 1981*a*, p. 59]).

In order to assist in estimating ρ for the population, we now obtain ρ as a function of D/L. Let us suppose, as shown in Fig. 1, that the shape of a crypt is roughly that of a cylinder with a hemispherical base of radius R (Bjerknes and Cheng, 1981*a*, p. 61). Consider a given crypt of length L with K cell columns round the crypt and let C be the number of cycling cells in the hemispherical base less the number of noncycling cells between the top of the base and D. As discussed above, we can equate the number of cells between D and ρD with the number of cycling cells below D, so that

$$\frac{K(\rho - 1)D}{d_v} = \frac{K(D - R)}{d_v} + C, \quad (13)$$

where d_v is the width parallel to the crypt axis of the basal projection of the crypt cells in the cylindrical portion of the crypt (see Fig. 1). Solving Eq. (13) for ρ gives

$$\rho = 2 - \frac{1}{D}\left[R - \frac{d_v C}{K}\right] = 2 - \eta\left(\frac{D}{L}\right)^{-1}, \quad (14)$$

where we have introduced

$$\eta = \left[\frac{R}{L} - \left(\frac{d_v}{L}\right)\left(\frac{C}{K}\right)\right] \tag{15}$$

which must be independent of v because ρ and D/L are independent of v (see Eq. [10]). For convenience we write ρ in terms of D_0 and L_0 as

$$\rho = 2 - \frac{\eta L_0}{d_v}\left(\frac{d_v}{D_0}\right). \tag{16}$$

(e) Relation Between the Distance x and Cell Position p. The index distributions measured experimentally are functions of cell position p and correspond to $\langle\Phi\rangle(p)$. To obtain $\langle\Phi\rangle(p)$ we need to transform the index distribution $\Phi(x; v)$ given in Eq. (7) into a function of p denoted $\Phi(p; v)$. This requires the mapping between x and p. As noted before, the relationship between x and p does not correspond simply to a change in units because of the hemispherical shape of the crypt base.

For convenience we define cell position p to be a continuous variable that specifies the number of complete cells and fraction of a cell situated below p, e.g., below p = 5.5 are 5½ cells. It should be noted that points between p = 0 and 1, p = 1 and 2, etc., correspond to what are usually referred to as cell position 1, cell position 2, etc., respectively. The crypt is again assumed cylindrical with a hemispherical base of radius R (see Fig. 1). Assuming the cut-off D is somewhere in the cylindrical region of the crypt, it is sufficient for our purposes to determine the mapping between x and p for $x \geq R$ only. Let the cell position p at $x = R$ be p_R. Then for $p \geq p_R$,

$$x = R + d_v(p - p_R) \tag{17}$$

which implies that for $x \geq R$,

$$p = \frac{x}{d_v} + \left(p_R - \frac{R}{d_v}\right), \tag{18}$$

where d_v is the cell width shown in Fig. 1. For simplicity we assume that d_v is independent of crypt volume and that p_R and R scale as $v^{1/3}$. Then the required transformation has the form

$$p = \frac{x}{d_v} + \delta v^{1/3}, \quad x \geq R \tag{19}$$

or equivalently

$$x = d_v(p - \delta v^{1/3}), \quad p \geq p_R, \tag{20}$$

where δ is a constant independent of crypt volume v and

$$\delta v^{1/3} = p_R - \frac{R}{d_v}. \tag{21}$$

The inhomogeneous term in the transformation between x and p given by Eq. (19) is due to the hemispherical shape of the crypt base. The presence of this term shifts the curve for $\langle\Phi\rangle(p)$ that would be obtained if $\delta = 0$ by roughly two cell positions in the direction of higher p in the rat ($\delta v^{1/3}$ for an average sized rat crypt is estimated to be 1.8; see Section IV[a]). Ignoring the hemispherical shape of the crypt base may therefore be the reason that the labeling index distribution predicted by Cairnie et al. (1965*b*, p. 549) using their slow cut-off model was shifted about two cell positions lower than the measured distribution. The volume dependence of the transformation between x and p means that a given position x corresponds to a range of cell positions p in the crypt population. Thus averaging over the crypt population at a fixed x to obtain $\langle\Phi\rangle(x)$ is not equivalent to averaging at a fixed p to obtain $\langle\Phi\rangle(p)$.

(f) Population Averaged Index Distributions. We now may average over the ensemble of volumes in the crypt population to obtain $\langle\Phi\rangle(p)$ as prescribed in Eq. (1). To do this we first obtain $\Phi(p; v)$ by rewriting Eq. (7), using Eqs. (10) and (20), in the form

$$\Phi(p; v) = \begin{cases} 0, & v < (p/\beta_p)^3 \\ 2\gamma_0\left(\dfrac{\Lambda}{d_v\delta}\right)^{\ln 2/\ln\rho}\left(\dfrac{p}{\delta v^{1/3}} - 1\right)^{-\ln 2/\ln\rho} - B, & \\ \quad (p/\beta_p)^3 < v < (p/\alpha_p)^3 & \\ A, & v > (p/\alpha_p)^3 \end{cases} \tag{22}$$

where

$$\Lambda = (D_0/V_0^{1/3}), \tag{23}$$

$$\alpha_p = \frac{\alpha_x\Lambda}{d_v} + \delta, \tag{24}$$

$$\beta_p = \frac{\beta_x\Lambda}{d_v} + \delta, \tag{25}$$

and $p \geq p_R$. Let p_R^{max} be the value of p_R for the crypt of largest size with $v = V_0 + \Delta V$. Provided we restrict ourselves to $p \geq p_R^{max}$, Eq. (22) holds for the entire range of volumes from V_0 to $V_0 + \Delta V$ so that Eq. (1) can be evaluated. The mathematical form of $\langle\Phi\rangle(p)$ is given in Appendix B.

The range of cell positions over which $\langle\Phi\rangle(p)$ is decreasing, r_p, is given by

$$r_p = p_4 - p_1 = \frac{D_0}{d_v}(\beta_x - \alpha_x) + (\theta - 1)\left[\frac{D_0}{d_v}\beta_x + \delta V_0^{1/3}\right] \tag{26}$$

using Eqs. (B7) and (B10), where p_1 is the position where $\Phi(p; V_0)$ begins to decrease and p_4 is the position where $\Phi(p; V_0 + \Delta V)$ just reaches 0. If all crypts had the same

volume, a situation corresponding to the original sharp cut-off model of Cairnie et al. (1965*b*), θ would equal 1 and only the first term of Eq. (26) would remain. The extra spread in the range of decrease of $\langle\Phi\rangle(p)$ due to the variability of crypt volume is therefore given by the second term of Eq. (26). In the case of the mitotic index, Cairnie et al. (1965*b*) concluded that what we call r_p was much too small if $\theta = 1$. For our model to be acceptable then, the second term of our Eq. (26) must make the dominant contribution to r_p when the α_x and β_x are those for the mitotic index. A quick check of this can be made by first noting that $\delta V_o^{1/3} > 0$ (see Section IV[*a*]) so that the second term of Eq. (26) is greater than $(\theta - 1)\rho D_o/d_v$ which is roughly (0.3) $\rho D_o/d_v$ in the mouse and (0.6) $\rho D_o/d_v$ in the rat (see Section IV). On the other hand, the first term is roughly (0.05) $\rho D_o/d_v$ in both the mouse and rat (as will be seen, $\gamma_o \sim 1$, $\rho \sim 2$, $\mu_o \sim 0.05$). Thus the dominant contribution to the range of cell positions over which the mitotic index is decreasing results from the pooling of crypts of different sizes.

(g) Model Parameters. Looking at Eqs. (B1) through (B13) and Table I, we see that the predicted index distributions, $\langle\Phi\rangle(p)$, depend upon 9 parameters: γ_o, λ_o, μ_o, T_s/T, ρ, θ, D_o/d_v, $\delta V_o^{1/3}$, and p_R^{max}. From Eq. (16) we see that ρ may in turn be specified in terms of $\eta L_o/d_v$ and the already mentioned D_o/d_v. In defining these parameters we have assumed, where applicable, that distances are measured in some physical length unit such as microns. It is convenient, however, to express the height of the cut-off in the smallest crypts in terms of the number of cell postitions which we denote by $\not\Phi_o$. This parameter may then be used in place of D_o/d_v since from Eq. (20)

$$D_o/d_v = \not\Phi_o - \delta V_o^{1/3}. \tag{27}$$

In what follows, the validity of our generalized sharp cut-off model was tested by comparing the predicted $\langle\Phi\rangle(p)$ with measured labeling and mitotic index distributions from the mouse and rat. The parameters $\not\Phi_o$, λ_o, μ_o for the mouse and $\not\Phi_o$, λ_o, μ_o, and θ for the rat were obtained by fitting $\langle\Phi\rangle(p)$ to the data. The remaining parameters of the model were held fixed at values estimated using data from the literature (see Sections III[*b*] and IV[*a*]).

III. MATERIALS AND METHODS

(*a*) Labeling and Mitotic Index Distributions

Distal jejunum from eight Swiss albino mice was processed for autoradiography and light microscopy as described in Cheng and Leblond (1974). The animals were raised under similar conditions and were approximately the same age and weight (26 to 35g). The animals were killed between 10 and 11 A.M. For each of 104 crypts, all the cells of a single cell column from an optimally oriented section were scored as being labeled or unlabeled and mitotic or not mitotic. A few cells were both labeled and mitotic. These were included in the determination of both the labeling and mitotic indices. Because of the range of crypt lengths (see Fig. 2 *a*), the total number of cells obtained at the higher cell positions decreases (we had a range of from 1 to 104 cells per position).

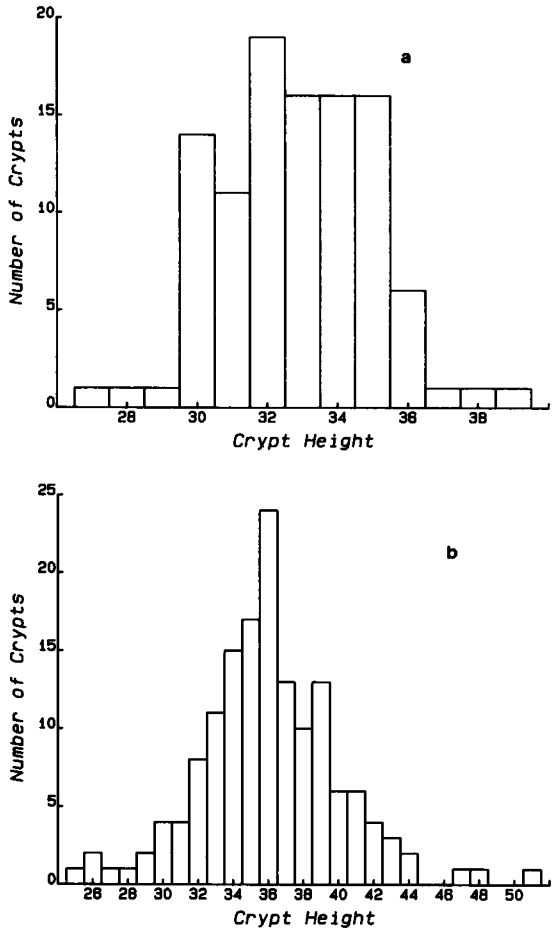

FIGURE 2 Distribution of observed jejunal crypt lengths (expressed in terms of cell positions). (*a*) Total of 104 crypts from mouse. (*b*) Total of 150 crypts from rat (data from Cairnie et al., 1965a).

For the rat, we used the published labeling and mitotic index distributions of Cairnie et al. (1965*a*, *b*). These measurements were for 150 crypts from the proximal jejunum of 8-wk old-male rats of the August strain (100 to 200 g). Reading the data points from the original figures was facilitated by the use of a digitizing tablet. The number of cells observed at a given position by Cairnie et al. (1965*a*) equals the number of crypts they considered of a height equal to or less than that given position. Their reported frequency of crypts as a function of height was therefore digitized (see Fig. 2 *b*) and the observed number of cells at a given height determined (from 101 to 150 cells per position for the labeling index data and from 60 to 150 cells per position for the mitotic index data).

(*b*) Parameter Estimation

To test the validity of Eq. (9) and determine the constant a, the lengths and volumes of crypts from mouse proximal jejunum were measured. The two lots (A and B) of five male Swiss albino CD-1 mice described in Totafurno et al. (1987, Section III[*e*]) were again used (28.5–29.5 g for group A and 32.0–33.7 g for group B). In Totafurno et al. (1987), a method for estimating the volumes of crypts from longitudinal outlines is described and the volume of 342 crypts in group A and 291 crypts in group B reported. We used the same volume data here. In addition, the length of the symmetry axis selected by the computer algorithm for each of these crypts was determined.

The parameters γ_o and T_s/T for both the mouse and rat and the parameter θ for the mouse were taken from the literature (see Section

IV[a]). No published value of θ for the rat was available so it was determined in the fit of the model to the rat index distribution data described below.

To determine the parameter $\eta L_o/d_v$ (see Section II[g]), we first note that under the assumption of a hemispherical crypt base, the radius

$$R = \frac{Kd_h}{2\pi}, \tag{28}$$

where K, as before, is the number of cell columns and d_h is the width perpendicular to d_v of the basal projection of crypt cells in the cylindrical portion of the crypt (see Fig. 1). Using Eqs. (15) and (28) we obtain

$$\frac{\eta L_o}{d_v} = \left(\frac{L_o}{\bar{L}}\right)\left[\frac{K}{2\pi}\frac{d_h}{d_v} - \frac{C}{K}\right], \tag{29}$$

where we have explicitly written the average crypt length $\bar{L}$ because the quantities in square brackets in Eq. (29) are presumed to be representative of a crypt of average length. It can be shown on the basis of Eqs. (9), (3), and (11) that

$$\left(\frac{L_o}{\bar{L}}\right) = \left(\frac{V_o}{\bar{v}}\right)^{1/3} = \left[1 + (\theta^3 - 1)\left(\frac{1}{\ln 2} - 1\right)\right]^{-1/3}, \tag{30}$$

where $\bar{v}$ is the average crypt volume. Thus $\eta L_o/d_v$ can be estimated given θ, K, d_h/d_v, and C.

It has already been assumed (see derivation of Eq. [19]) that p_R and R scale as $v^{1/3}$ so that

$$p_R^{max} = \bar{p}_R\left(\frac{V_o + \Delta V}{\bar{v}}\right)^{1/3} = \bar{p}_R\theta\left(\frac{V_o}{\bar{v}}\right)^{1/3} \tag{31}$$

and

$$\delta V_o^{1/3} = \left(\bar{p}_R - \frac{\bar{R}}{d_v}\right)\left(\frac{V_o}{\bar{v}}\right)^{1/3}, \tag{32}$$

(see Eq. [21]) where the bar indicates the value of the quantity for a crypt of average volume. Now $\bar{R}$ and $(V_o/\bar{v})^{1/3}$ are given by Eqs. (28) and (30), respectively. Thus p_R^{max} and $\delta V_o^{1/3}$ can be estimated given θ, K, d_h/d_v, and C.

The remaining parameters Ψ_o, λ_o, and μ_o for the mouse and Ψ_o, λ_o, μ_o, and θ for the rat were obtained using a maximum likelihood fit of the model (Eqs. [B1] to [B13]) to the measured labeling and mitotic index distributions. The fit was restricted to positions $p \geq 10$ in the mouse and $p \geq 7$ in the rat.[4] The likelihood function and the manner in which the data were binned are reported in Section III(c). Both the best values for these index distributions individually and the overall best value were computed using the minimization routine MINUIT (C.E.R.N.).

(c) Comparison of Fitted Model to the Data

In comparing our fitted model to the data, we used the likelihood ratio test as follows (see Kalbfleisch, 1985, Section 12.4 and Mood et al., 1974, Section IX 5.1). Let $\hat{\Phi}_i$ and Φ_i be the observed and predicted value, respectively, of the index distributions at cell position i. Here

$$\Phi_i = \int_{i-1}^{i} \langle\Phi\rangle(p)\, dp, \tag{33}$$

where $\langle\Phi\rangle(p)$ is given by the model. Also let n_i be the number of cells sampled at cell position i. Then $\hat{r}_i = n_i\hat{\Phi}_i$ and $r_i = n_i\Phi_i$ are the number of labeled (or mitotic) cells observed and predicted, respectively, at cell position i. We assume that the number of labeled (or mitotic) cells observed, $\hat{r}_i$, is binomially distributed with probability Φ_i that a single cell selected from position i is labeled (or mitotic). We also assume that the $\hat{r}_i$ for different cell positions i are statistically independent (this is not strictly true for our data because all cells in a given column are included in the determination of the index distribution thus rendering the sampling process nonrandom). The likelihood function is then

$$\mathcal{L}_{|n_i;\hat{r}_i|}(\Phi_i|\Psi_o, \lambda_o, \mu_o, \theta) = \prod_i \binom{n_i}{\hat{r}_i}\Phi_i^{\hat{r}_i}(1 - \Phi_i)^{n_i - \hat{r}_i}. \tag{34}$$

The test statistic we used was the negative log likelihood ratio statistic defined as

$$D = -2 \ln [\mathcal{L}(\Phi_i)/\mathcal{L}(\Phi_i = \hat{\Phi}_i)]. \tag{35}$$

It can be shown (Fraser, 1976) that D is approximately χ^2 distributed with the number of degrees of freedom equal to the number of Φ_i less the number of parameters fitted to the index distribution data. To ensure that D is χ^2 distributed, we chose to pool the data at the higher cell positions (where data is sparse) into a single bin j with $\hat{r}_j$, $n_j - \hat{r}_j$, r_j, and $n_j - r_j$ all greater than or equal to 2. It was convenient in evaluating the likelihood function to also pool the data in this way (see Section V[e]). The comparison of the model to the data was restricted to positions $p \geq 10$ in the mouse and $p \geq 7$ in the rat.

IV. RESULTS

(a) Parameters Determined Independently of Index Distributions

The equation $L = av^b$, where L is crypt length, v is crypt volume, and a and b are fitted constants, was found to fit the data with a correlation coefficient of 0.507 ($P < 0.001$, $dF = 340$) for the mice of group A and 0.530 ($P < 0.001$, $dF = 289$) for the mice of group B. The 95% confidence limits on b were 0.229 to 0.330 for group A and 0.256 to 0.372 for group B. The value $b = 1/3$ as used in Eq. (9) therefore lies well within the 95% confidence limits on b for group B and only slightly outside of the comparable limits for group A suggesting that $b = 1/3$ is not an unreasonable approximation. Fitting $L = av^{1/3}$ to both sets of data yields $a \approx 2.5$.

Since the average growth fraction distribution appears to reach a peak value of ~1 for both the mouse and rat (Fig. 17.8 of Wright and Alison, 1984), γ_o was taken to be 1. As representative values of T_s/T for the mouse and rat, we used 0.59 (Table 18.3 of Wright and Alison, 1984) and 0.62 (Table II of Cairnie et al., 1965a), respectively. An average value of $\theta = 1.32$ was obtained for the mouse from Totafurno et al. (1987, Table IV).

The value of d_h/d_v used for the mouse was 0.95 (Bjerknes and Cheng, 1981a). Due to a lack of data, the

[4]Here we are concerned with predicting the decrease in the index distributions that occurs above the cut-off. These predictions are dependent in only a coarse-grained way upon the index distributions below the cut-off through the parameter C, the total number of cycling cells in the hemispherical base less the number of noncycling cells between the top of the base and the cut-off (see Eqs. [14] and [15]). We could therefore ignore the observed decrease in the index distributions that occurs towards the bottom of the crypt for reasons beyond the scope of our model. In comparing the model to the data we restricted ourselves to positions above a point where the index distributions appeared to level off.

same value of d_h/d_v was used for the rat. The column count K we used was 18.7 for the mouse (Bjerknes and Cheng, 1981*a*) and 24.5 for the rat (Wimber and Lamerton, 1963). Direct measurements of $\bar{p}_R$ and C were not available. However, estimates of $\bar{p}_R$ and C (see Bjerknes and Cheng, 1981*a*; Cairnie, 1970) indicate that $\eta L_o/d_v$ (as determined by Eqs. [29] and [30]) is small enough that ρ is roughly 2 in both the mouse and rat for the expected ranges of Φ_o and θ (see Eqs. [16] and [27]). For simplicity we therefore set $\rho = 2$ in both the mouse and rat. In evaluating p_R^{max} and $\delta V_o^{1/3}$ (see Eqs. [31] and [32]), the value of $\bar{p}_R$ used was 4 in the mouse and 5.5 in the rat. These values yield $p_R^{max} = 4.5$ and $\delta V_o^{1/3} = 1.0$ for the mouse and $p_R^{max} = (5.5)\ \theta(V_o/\bar{v})^{1/3}$ and $\delta V_o^{1/3} = (1.8)\ (V_o/\bar{v})^{1/3}$ for the rat, where $(V_o/\bar{v})^{1/3}$ is given by Eq. (30) (as reported below, we found $\theta = 1.64$ in the rat so that $p_R^{max} = 6.6$ and $\delta V_o^{1/3} = 1.3$). For a crypt of average volume $\bar{v}$, the inhomogeneous term in the transformation between x and p given by $\delta\bar{v}^{1/3}$ (see Eq. [19]) has the value 1.2 in the mouse and 1.8 in the rat (see Eq. [32]).

(*b*) Fitting the Model to the Index Distribution Data

We begin with the maximum likelihood estimates found for Φ_o, λ_o, and μ_o in the mouse (each estimate is followed in brackets by a range of values indicating the 95% confidence interval). The best fit of the model was obtained for the labeling index data alone, the mitotic index data alone, and for both sets of data simultaneously (we refer to this last fit as the combined fit). We found that for the labeling index fit $\Phi_o = 13.4$ (12.5 to 14.2) and $\lambda_o = 0.55$ (0.51 to 0.59); for the mitotic index fit $\Phi_o = 12.0$ (11.4 to 12.8) and $\mu_o = 0.055$ (0.041 to 0.071); and for the combined fit $\Phi_o = 12.7$ (12.3 to 13.5), $\lambda_o = 0.51$ (0.505 to 0.55), and $\mu_o = 0.050$ (0.037 to 0.067). The estimated values of λ_o were consistent with the values of T_s/T and γ_o used (for $T_s/T = 0.59$ and $\gamma_o = 1$, $0.505 \le \lambda_o \le 0.671$; see Eq. [8]). In each of these cases, there was no significant difference between the model and the data at the 5% level. Fig. 3 shows the predicted distributions for the combined fit together with the data points.

For the rat, we obtained the maximum likelihood estimates for Φ_o, λ_o, μ_o, and θ. For simplicity, θ was estimated first using a combined fit to the labeling and mitotic index distributions and found to be $\theta = 1.64$ with 95% confidence limits of 1.39 to 1.92. Then with θ held fixed at this value, estimates of Φ_o, λ_o, and μ_o were made as was done for the mouse. We found that for the labeling fit $\Phi_o = 11.9$ (11.4 to 12.3) and $\lambda_o = 0.63$ (0.60 to 0.66); for the mitotic index fit $\Phi_o = 10.4$ (9.9 to 11.1) and $\mu_o = 0.061$ (0.049 to 0.073); and for the combined fit $\Phi_o = 11.5$ (11.0 to 12.0), $\lambda_o = 0.61$ (0.58 to 0.64) and $\mu_o = 0.053$ (0.042 to 0.066). Again the estimated values of λ_o were consistent with the values of T_s/T and γ_o used (for $T_s/T = 0.62$ and $\gamma_o = 1$, $0.537 \le \lambda_o \le 0.699$; see Eq. [8]). For each of these fits, there was no significant difference between the model and the data at the 5% level. Fig. 4 shows the predicted distributions for the combined fit with $\theta = 1.64$ together with the measured data points.

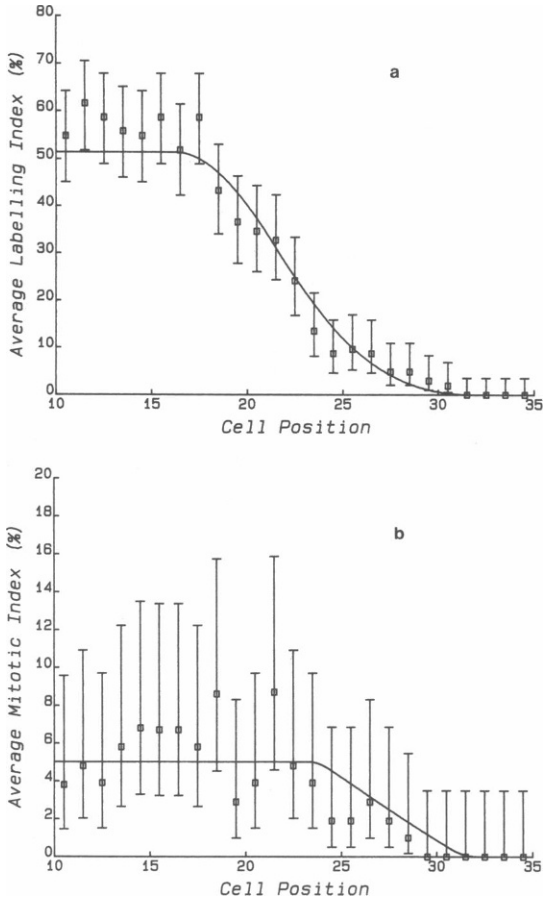

FIGURE 3 Average labeling and mitotic index distributions (defined as the number of labeled or mitotic cells, respectively, at a given position divided by the number of crypts sampled) as a function of cell position (p) for the mouse. The observed values are indicated by the points; error bars correspond to the 95% confidence limits on these frequencies assuming binomial sampling error (see Section 4.7 of Lloyd, 1984). The solid curves indicate the predictions of the model as given by Eqs. (B1) through (B6) using the maximum likelihood estimates of the 3 parameters Φ_o, λ_o, and μ_o obtained in the simultaneous fit of the model to both the labeling and mitotic index distribution data. The parameter values are $\gamma_o = 1$, $T_s/T = 0.59$, $\rho = 2$, $\theta = 1.32$, $\delta V_o^{1/3} = 1.0$, $p_R^{max} = 4.5$, $\lambda_o = 0.51$, $\mu_o = 0.050$, and $\Phi_o = 12.7$. (*a*) Average labeling index. The positions given by Eqs. (B7) through (B10) are $p_1 = 16.3$, $p_2 = 24.0$, $p_3 = 21.5$, and $p_4 = 31.6$. (*b*) Average mitotic index. Here $p_1 = 23.2$, $p_2 = 24.4$, $p_3 = 30.7$, and $p_4 = 32.2$.

As $\theta \to 1$, variation of crypt size in the model is suppressed and our model corresponds to the sharp cut-off model of Cairnie et al. (1965*b*). We repeated the above anlaysis for both the mouse and rat with $\theta = 1.01$. Because of the large error bars on the mitotic index data (see Figs. 3 and 4), when the model with $\theta = 1.01$ was compared with the mitotic index data alone, no statistically significant difference was obtained at the 5% level for both the mouse and rat. In contrast, when the model with $\theta = 1.01$ was

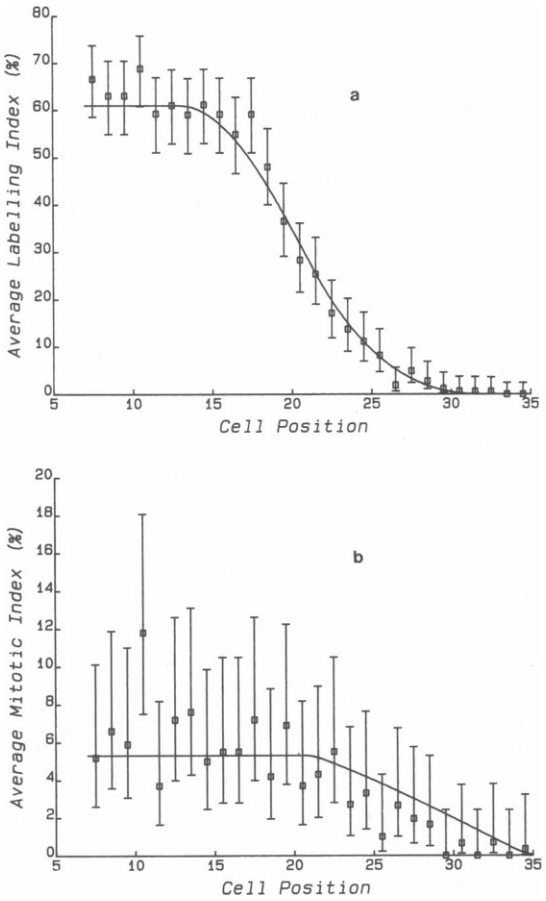

FIGURE 4 Average labeling and mitotic index distributions as a function of cell position (p) as in Fig. 3 except now for the rat. The index distribution data are taken from Cairnie et al. (1965*a*, *b*). The maximum likelihood estimates for the 4 parameters θ, Φ_o, λ_o, and μ_o obtained in the simultaneous fit of the model to both the labeling and mitotic index distribution data are used. The parameter values are $\gamma_o = 1$, $T_s/T = 0.62$, $\rho = 2$, $\theta = 1.64$, $\delta V_o^{1/3} = 1.3$, $p_R^{max} = 6.6$, $\lambda_o = 0.61$, $\mu_o = 0.053$, and $\Phi_o = 11.5$. (*a*) Average labeling index. The positions given by Eqs. (B7) through (B10) are $p_1 = 13.0$, $p_2 = 19.3$, $p_3 = 21.3$, and $p_4 = 31.6$. (*b*) Average mitotic index. Here $p_1 = 20.6$, $p_2 = 21.7$, $p_3 = 33.9$, and $p_4 = 35.5$.

compared with the labeling index data alone or with the labeling and mitotic index data simultaneously, there was a significant difference in both mouse and rat. Thus the sharp cut-off model is unacceptable if the variation in crypt size is neglected. Since the essential effect of letting $\theta \to 1$ in our model is to suppress variation in the height of the cut-off, these results also indicate the unacceptability of a model in which the height of the cut-off is in some way fixed irrespective of crypt size.

V. DISCUSSION

(*a*) Crypt Population Inhomogeneity and a Reassessment of the Standard Model

The observed labeling and mitotic index distributions of intestinal crypts are interpreted by the standard slow cut-off model (Cairnie et al., 1965*b*) as indicating a gradual cessation of proliferation at higher positions within individual crypts. Here, we have considered an alternative interpretation that explicitly incorporates crypt size variation. For crypts of a given size, the index distributions are computed assuming that the transition between the proliferative and nonproliferative compartments occurs over as few positions as is biologically tenable (the sharp cut-off model of Cairnie et al., 1965*b*). Then the index distributions for the entire crypt population are obtained by averaging over the ensemble of crypt volumes. We have shown in a quantitative fashion that the predictions of this model are consistent with existing data. Our conclusion is therefore that a sharp transition in the proliferative state of cells within the crypt cannot be ruled out at present.

(*b*) Population Averaged Index Distributions

Variation in crypt size (see Fig. 2) makes the definition of the average index distributions somewhat subtle because at higher positions the number of cells sampled is smaller than the number of crypts sampled. In the usual sampling process, the index distribution is defined relative to the number of cells actually sampled at a given position; however, as shown below, the use of this definition requires that the model include an additional parameter. We have therefore found it convenient to redefine the average index distribution at a given position to be the number of labeled (or mitotic or cycling) cells expected at that position divided by the total number of crypts sampled. Eq. (1) conforms to this definition because $1 - \langle\Phi\rangle(p)$ is the probability that a sampled crypt has either an unlabeled, (or nonmitotic or noncycling) cell at p, or no cell at all at p. These two definitions for the average indices become identical for positions below the length of the shortest crypts, L_o, because at these positions the number of cells sampled equals the number of crypts sampled. The values of λ_o, μ_o, and γ_o are therefore the same using either definition.

The average index distributions using either definition are the same for positions below $x = L_o$ (as mentioned above) and for positions above $x = L_{max}$ (where they are identically 0). Between $x = L_o$ and $x = L_{max} - \theta L_o$ (see Eq. [11]), the two definitions give different distributions that can be transformed, however, into one another as follows. Let the volume of a crypt whose length is p be v_p. A crypt will have a cell at position p if its volume $v \geq v_p$. The usual definition of the index distribution at a given position p is really the conditional probability of finding a labeled (or mitotic or cycling) cell at that position given that the selected crypt has $v \geq v_p$. On the other hand, the average index distribution $\langle\Phi\rangle(p)$ used here is actually the joint probability that a selected crypt has a labeled cell at p and has $v \geq v_p$ (the presence of a labeled cell at p automatically implies $v \geq v_p$). By the definition of conditional probability we therefore may obtain index distributions conforming to

the usual definition by dividing $\langle\Phi\rangle(p)$ by the probability distribution function $F(v_p)$, given by (see Eq. [2])

$$F(v_p) = \int_{v_p}^{V_o+\Delta V} f(v)\,dv, \tag{36}$$

where $V_o < v_p < V_o + \Delta V$ (or equivalently, $L_o < x < \theta L_o$). From Eqs. (9) and (20) we find that

$$v_p = p^3 \Big/ \left(\frac{a}{d_v} + \delta\right)^3. \tag{37}$$

Let the length in cell positions corresponding to the length $x = L_o$ be

$$L_o^p = L_o/d_v + \delta V_o^{1/3} \tag{38}$$

(see Eq. [19]). Then evaluating Eq. (36) using Eqs. (2), (9), and (11) gives F as a function of p

$$F(p) = 2\exp\left\{\left[-\frac{\ln 2}{\theta^3 - 1}\right]\left[\left(\frac{p}{L_o^p}\right)^3 - 1\right]\right\} - 1, \tag{39}$$

where $L_o^p < p < \theta\, L_o^p$. Thus the probability of obtaining a labeled, mitotic, or cycling cell at p expressed relative to the number of cells samples at p is

$$\begin{cases} \langle\Phi\rangle(p), & \text{if } p \le L_o^p \\ \langle\Phi\rangle(p)/F(p), & \text{if } L_o^p < p < \theta L_o^p, \\ 0, & \text{if } p \ge L_o^p \end{cases} \tag{40}$$

where L_0^p and $F(p)$ are given by Eqs. (38) and (39), respectively.

The expression Eq. (40) involves the additional parameter L_o^p (or equivalently L_o/d_v; see Eq. [38]). Rather than including this additional parameter in the model, we have chosen to introduce the new method of presenting the results described above. Another difference between the new and old methods of defining the average index distributions is that the binomial sampling error at the higher positions is reduced under the new definition used here. This is because under our definition the relevant number of samples at a given position is the total number of crypts selected, while under the old scheme the relevant number of samples is the number of crypts with a cell in that position.

(c) Mitotic Index Distribution and Sampling Error

It has not generally been recognized in the literature that the relative binomial sampling error in the measurement of a low frequency such as the mitotic index can be large unless sufficient numbers of crypts are sampled (see confidence limit table for the binomial parameter in Pearson and Hartley, 1966). In fact little confidence can be placed in the detailed form of published mitotic index distributions. As shown in Figs. 3 and 4, the 95% confidence limits on the measured mitotic index at any given position is roughly of the order of the index itself. To obtain relative errors of a size similar to that of the labeling index measurements will require increasing the number of crypts sampled to ~500 (Pearson and Hartley, 1966). Such improvement in the precision of the mitotic index measurements would permit a much more stringent test of our generalized sharp cut-off model.

(d) Parameter Estimates

The model we have proposed involves 9 parameters as listed in Section IV(a). In predicting the form of the labeling and mitotic index distributions in the mouse, however, only three of these parameters were determined by fitting to the labeling and mitotic index distributions themselves. The other parameters were estimated independently of the index distributions using data from the literature. In particular, an independent measurement of the degree of variability in crypt size, specified by the parameter θ in the model, was used for the mouse. Unfortunately, for the rat, no such estimate of θ was available in the literature. Since there was significantly greater variability in the observed distribution of crypt lengths for the rat than for the mouse (see Fig. 2), the value of θ estimated from the rat index distribution data was probably not unduly large.

From Eq. (11) we see that crypts vary in length from a minimum length $L = L_o$ in crypts with volume V_o to a maximum length $L = \theta L_o$ in crypts of volume $V_o + \Delta V$. Accordingly, the cut-off position $\Phi(v)$ varies from Φ_o in the smallest crypts to $\theta\Phi_o$ in the largest crypts (from Eqs. [11], [12], and [20]). For the mouse, $\Phi(v)$ was estimated to vary from $\Phi(V_o) = \Phi_o = 12.7$ (12.3 to 13.5; 95% confidence limits) to $\Phi(V_o + \Delta V) = 16.7$. Similarly for the rat, we found that $\Phi(v)$ varied from $\Phi(V_o) = \Phi_o = 11.5$ (11.0 to 12.0; 95% confidence limits) to $\Phi(V_o + \Delta V) = 18.9$. Expressing these results in terms of cell position, we have found that with increasing crypt size from smallest to largest, the location of the cut-off in mouse jejunal crypts ranges from the thirteenth to the seventeenth cell position and in rat jejunal crypts from the twelfth to the nineteenth cell position.

A check of the consistency of these estimates for Φ_o can be made as follows. Assuming that the region between the cut-off D and the top of the proliferative zone ρD is cylindrical and that the number of cell columns is K, then the total number of cycling cells in the crypt is given by

$$\frac{K(\rho - 1)D}{d_v} + \frac{K}{d_v}\int_D^{\rho D} \gamma(x)\,dx, \tag{41}$$

where the first term is taken from Eq. (13) and $\gamma(x)$ is given by Eq. (7). Since $\rho \sim 2$ and $\gamma_0 \sim 1$, we find that the

total number of cycling cells in a crypt of average volume is approximately equal to

$$2 \ln 2 \, K \frac{D}{d_v} = 2 \ln 2 \, K \frac{D_0}{d_v} \left(\frac{\bar{v}}{V_0} \right)^{1/3} = 2 \ln 2 \, K (\not{D}_0 - \delta V_0^{1/3}) \left(\frac{\bar{v}}{V_0} \right)^{1/3} \quad (42)$$

where we have used Eqs. (10) and (20) to express this estimate in terms of $\not{D}_0$. Evaluating this expression using the parameters in Section IV and Eq. (30), we find that for the mouse the total number of cycling cells in an average sized crypt is ~353 cells which compares well with the measured average of 310 cycling cells per crypt (Table II of Cheng and Bjerknes, 1983). Thus $\not{D}_0 = 12.7$ implies that the average number of cells in a crypt, assuming an overall growth fraction for the mouse crypt of between 0.51 and 0.6 (Wright and Alison, 1984; Table II of Cheng and Bjerknes, 1983), is roughly 600 to 700 cells. This is consistent with the measured average number of cells per crypt of 609 ± 50.5 cells (Table I of Cheng and Bjerknes, 1983). Similarly for the rat, $\not{D}_0 = 11.5$ implies that the average number of cells per crypt is roughly 785 cells (the overall growth fraction was taken to be 0.6 for the rat crypt; Wright and Alison, 1984) which is probably consistent with the somewhat larger value of 849 cells obtained by Wimber and Lamerton (1963) since, as they suggest, their measurement included some surface epithelium.

The labeling and mitotic index data were sufficient to determine the position of the cut-off $\not{D}_0$ to within a couple of cell positions as shown by the 95% confidence limits quoted above. However these confidence limits are presumably underestimates since they do not incorporate any uncertainty in the value of the independently determined parameters listed in Section IV(*a*). Furthermore, no attempt has been made in the measurement of the labeling and mitotic indices to correct for selection artifacts such as those related to crypt size variability or that corrected by means of Tannock's factor (Wright and Alison, 1984). Therefore the estimated values of λ_0 and μ_0 should not be taken as the absolute frequencies for the crypt. Because the model is not strictly linear in λ_0 and μ_0, a uniform rescaling of the labeling index distribution and of the mitotic index distribution in an attempt to obtain absolute frequencies may alter the estimated value of $\not{D}_0$. We expect the effect of $\not{D}_0$ to be slight, however.

(*e*) Further Testing of the Model

Confidence in the estimated values of $\not{D}_0$ and in the model generally would be enhanced by improving the precision of the mitotic index measurements, as discussed in Section *V*(*c*) above. Nonetheless, the model was consistent at the 5% level with the relatively stringent labeling index data alone. We have yet to test how well the model predicts the growth fraction distribution. If the model predictions involving four fitted parameters (γ_0, λ_0, μ_0, and $\not{D}_0$) were simultaneously consistent with the labeling index, mitotic index, and growth fraction distributions, confidence in the model would be significantly increased, provided of course that the method of measuring the growth fraction distribution was independent of the labelling and mitotic index distributions.

The goodness of fit between the model and the data is expected to improve if the following two items ignored here were taken into account by the model. First, the labeling index at any given position was determined 1 h after administration of the radioisotope. In this time, cells initially labeled at one position have moved to higher cell positions by an amount which varies up the crypt reaching displacements of roughly one cell position (Cairnie et al., 1965*a*). Thus as pointed out by Cairnie et al. (1965*b*), the experimentally determined labeling index distribution is stretched somewhat to higher positions as compared with the distribution predicted by the model. In contrast, the mitotic index distribution data does not suffer such a measurement artifact. This may explain why the value of $\not{D}_0$ estimated by a fit to the labeling index distribution data alone was larger, in both the mouse and rat, than the value of $\not{D}_0$ estimated by a fit to the mitotic index distribution data alone. Secondly, we have included only binomial sampling error in the model and neglected other possible sources of error. In particular, we have neglected any error in the assignment of cell position. Such errors are cumulative with height so that their effect on the measured index distributions is most pronounced at just those positions where these curves are going to zero. This, we expect, is the reason for the measured curves having extended tails as compared with the predicted curves. In the maximum likelihood parameter estimation discussed in Section III(*b*), we avoided this discrepancy between the model and the data by combining the data in the tail of the distribution into a single bin.

We have identified the variation of crypt volume or equivalently crypt length within the crypt population as a major contributor to the apparent gradualness of the decrease in the labeling index, mitotic index, and growth fraction distributions. The corresponding distributions for crypts of a fixed length would therefore be expected to conform to the predicted distributions of the sharp cut-off model given by Eq. (22). This is in contrast to the slow cut-off model which would still predict that the index distributions for crypts of a given length decrease gradually with cell position. We did not attempt this direct test of the sharp cut-off model using our data for the mouse because the number of crypts obtained at any given length was small (<20) thus making the precision of estimates of the labeling or mitotic index distributions for a crypt of fixed length poor. To get enough crypts of a single length to obtain a degree of precision comparable to that of the labeling index distribution reported here (see Fig. 3) will

require sampling roughly 500 crypts for the labeling index distribution and 2,500 crypts for the mitotic index distribution.

The sharp cut-off index distributions given by Eq. (22) are identical for crypts of different size (see Eqs. [9] and [19]) when expressed as functions of position divided by length (i.e., as functions of $x/L(v)$ or p divided by length in cell positions). Thus averaging over the crypt population should in principle still yield the sharp cut-off model index distributions provided position is specified relative to crypt length. Our model therefore gives some justification for the normalizing scheme mentioned in the Introduction (Cairnie and Bentley, 1967; Wright et al., 1972). However, their procedure has the difficulty that upon normalization, positions from crypts of different lengths overlap. The pooling of the data into arbitrarily defined cell positions that is therefore required is done without justifying the implicit weighting used for the data from different sized crypts (a weighting which is inappropriate if our model is correct) and without analyzing the implications of this procedure upon the error estimates for the pooled data points. Furthermore, their technique is particularly sensitive to error in the cell position based length measurement which, as already explained, is expected to be relatively large.

(*f*) Biological Significance

This paper raises the spectre that much of our current understanding of the detailed kinetic organization of individual intestinal crypts is incorrect or at least without adequate justification. For example, the labeling and mitotic index distributions of intestinal crypts have been interpreted as indicating a slow spatial cut-off in the cessation of proliferation within the crypt (Cairnie et al., 1965*b*). We have shown, however, that these distributions can equally be explained by combining the simpler sharp spatial cut-off of proliferation within individual crypts with the effects of averaging over an inhomogeneous crypt population. In our view, current measurements would be better interpreted as ensemble averages over populations of inequivalent crypts varying widely in size (see Totafurno et al., 1987).

If corroborated by further testing, our work has important implications for models of crypt cell kinetics and the search for the underlying biological control mechanisms. It suggests that the signal to stop proliferation within an individual crypt occurs over a narrow range of positions within the crypt. This band of cell positions at D may also be where the maturation phase of crypt epithelial cell development is triggered. Although perhaps only coincidental, we have previously found in mouse duodenal crypts a narrow band of alkaline phosphatase activity at about the same point as the cut-off estimated here (Bjerknes and Cheng, 1981*c*).

VI. CONCLUSIONS

(*a*) Extant cell kinetic data is consistent with a sharp spatial transition between the proliferative and nonproliferative compartments of intestinal crypts. In contrast to the standard model of Cairnie et al. (1965*b*), we have proposed a generalized sharp cut-off model that explicitly incorporates the variation of crypt size in the crypt population. (*b*) Detailed models of intestinal epithelial cell renewal must incorporate the averaging over the ensemble of crypt volumes implicit in many measurements. (*c*) Little confidence can be placed in the details of the currently available mitotic index distributions. New measurements are needed along the lines proposed in Section V(*c*). (*d*) The sharp cut-off point in the jejunal crypts of the animals considered here ranges, depending upon crypt size, from roughly the thirteenth to the seventeenth cell position in mouse and from roughly the twelfth to the nineteenth cell position in rat. (*e*) Ignoring the geometry of the crypt base erroneously shifts the predicted labeling index, mitotic index, and growth fraction distributions towards higher cell positions by a significant amount (roughly two cell positions in the case of the rat) (see Section II[*e*]). Given the nature of the model, the necessity of incorporating the geometry of the crypt base could be avoided by measuring the index distributions with respect to absolute distance from the crypt base (i.e., x) rather than with respect to cell position (i.e., p). Besides decreasing the number of parameters in the model by 2, a further advantage of measuring the index distributions with respect to x rather than p is that x can be measured with greater precision than p especially at higher positions within the crypt where the index distributions are decreasing (see Section V[*e*]). The index distributions expressed as functions of x do not have the same form as those expressed as functions of p (see Section II[*e*]).

APPENDIX A

List of Symbols

- a See Eq. (9).
- A See Eq. (7) and Table I.
- α_p See Eq. (24).
- α_x See Eq. (7) and Table I.
- b Exponent in equation relating L to v (Section IV[*a*]).
- B See Eq. (7) and Table I.
- β_p See Eq. (25).
- β_x See Eq. (7) and Table I.
- C Number of cycling cells below R less the number of noncycling cells between R and D for crypts of average volume (Section II[*d*]).
- d_h, d_v See Fig. 1.
- D Location of cut-off within crypt in absolute distance units. Function of volume v (Section II[*c*], Eq. [10]).
- $D_o, \mathbb{D}_o$ Value of D for crypts of smallest volume V_o in terms of absolute distance units (Eq. [10]) and number of cell positions (Section II[g]), respectively.
- $\mathcal{D}$ Negative log likelihood ratio statistic (Eq. [35]).

ΔV Difference between the maximum and minimum crypt volumes in the population (Section II[b]).

$\delta v^{1/3}$ Inhomogeneous term in transformation between x and p (Eq. [19]).

η See Eq. (15).

$f(v)$ Probability density of crypt having volume v (Eq. [2]).

F Probability distribution function corresponding to $f(v)$. Function of v_p or p (see Eqs. [36] and [37]).

γ Growth fraction. Function of $(x; v)$ or $(p; v)$ (Section II[a]). $\gamma = \gamma_o$ at $D(v)$ (Section II[c]).

K Mid-crypt column count for crypt of average volume (Section II[d]).

$\mathcal{H}$ See Eq. (B12).

κ See Eq. (B11).

L Crypt length in absolute distance units. Function of volume v (Eq. [9]).

L_o, L_o^p Value of L for crypts of smallest volume V_o in absolute distance units (Eq. [9]) and in number of cell positions (Eq. [38]), respectively.

$\bar{L}$, L_{max} L for crypts of average volume $\bar{v}$ (Section III(b)) and largest volume $V_o + \Delta V$ (Section II[d]), respectively.

$\mathcal{L}$ Likelihood function as defined by Eq. (34).

λ Labeling index. Function of $(x; v)$ or $(p; v)$ (Section II[a]). At $D(v)$, $\lambda = \lambda_o$ (Section II [c]).

Λ See Eq. (23).

μ Mitotic index. Function of $(x; v)$ or $(p; v)$ (Section II[a]). At $D(v)$, $\mu = \mu_o$ (Section II[c]).

n_i Number of cells sampled at cell position i (Section III[c]).

p Position within crypt in number of cell positions as defined in Section II(e).

p_1 Cell position given by Eq. (B7) at which index distribution begins to decrease.

p_2, p_3 Cell positions given by Eqs. (B8) and (B9), respectively.

p_4 Cell position given by Eq. (B10) at which index distribution has decreased to 0.

p_R Cell position p corresponding to $x = R$ at top of hemispherical base of crypt. Function of volume v (Section II[e]).

$\bar{p}_R$, p_R^{max} p_R for crypts of average volume $\bar{v}$ (Section III [b]) and maximum volume (Eq. [31]), respectively.

$P(\sigma)$ Probability density for a cell at D being a cycling cell with phase σ (Eq. [4]).

Φ Index distributions λ, μ, or γ. Functions of $(x; v)$ or $(p; v)$ (Section II[a]).

$\langle\Phi\rangle$ Average of Φ over the distribution of crypt volumes. Defined at each position as the expected number of labeled, mitotic or cycling cells at the given position divided by the total number of crypts sampled (see Section V[b]). Function of x or p; however, $\langle\Phi\rangle(x)$ is not equivalent to $\langle\Phi\rangle(p)$ (Sections II[b], [e]).

Φ_i, $\hat{\Phi}_i$ Predicted and observed values of index distribution, respectively, for cell position i (Eq. [33]).

r_i, $\hat{r}_i$ Predicted and observed number of labeled (or mitotic) cells, respectively, for cell position i (Section III[c]).

r_p Range of cell positions over which index distribution decreases (Eq. [26]).

R Radius of hemispherical base of crypt (Fig. 1). Function of volume v. $R = \bar{R}$ for crypt of average volume $\bar{v}$ (Section III[b]).

ρ Top of proliferative zone is at $x = \rho D$ (Section II[c]).

σ Phase of cell cycle (Section II[c]).

σ_{min} Minimum phase of cells at a position x between D and ρD (Section II[c]). Function of x.

t Time, or age of cell (Section II[c]).

T Cell cycle time (Section II[c]).

T_s Duration of S-phase of the cell cycle (Section II[c]).

θ Ratio of maximum to minimum crypt length (Eq. [11]).

Υ See Eq. (B13).

v Crypt volume (Section II[a]). $\bar{v}$ is average crypt volume (Eq.[3]).

v_p Volume of crypt with length p (Eq. [37]).

V_0, $V_0 + \Delta V$ Minimum and maximum crypt volumes, respectively, in the population (Section II[b]).

x Position within crypt in absolute units such as microns (Section II[a]).

APPENDIX B

Expressions for the Population Averaged Index Distributions

As explained in Section II(f), we obtain the population averaged index distributions $\langle\Phi\rangle(p)$ by evaluating Eq. (1) with $\Phi(p; v)$ given by Eq. (22) for $p \geq p_R^{max}$. Depending upon the value of p, the three different forms of $\Phi(p; v)$ given in Eq. (22) will be used to varying extents in integrating over V_o to $V_o + \Delta V$. For a given index distribution, let the positions in the smallest crypts of volume V_0 where $\Phi(p; v)$ begins to decrease and where $\Phi(p; v)$ just reaches 0 be denoted by p_1 and p_2, respectively. Similarly, let the positions in the largest crypts of volume $V_o + \Delta V$ where $\Phi(p; v)$ begins to decrease and where $\Phi(p; v)$ just reaches 0 be denoted by p_3 and p_4, respectively. Substituting Eqs. (22) and (2) into Eq. (1) and using Eqs. (23), (24), (25), and (11), the integration then yields one of the following six distinct forms depending upon the value of p:

(i) $$\langle\Phi\rangle(p) = A, \quad \text{if } p_R^{max} < p < p_1 \tag{B1}$$

(ii) $$\langle\Phi\rangle(p) = \mathcal{H}\Upsilon\left(\kappa, \kappa\left(\frac{p}{p_1}\right)^3\right) - (2B + A) + 2(B + A)e^{\kappa}\exp\left[-\kappa\left(\frac{p}{p_1}\right)^3\right],$$
$$\text{if } p_1 < p < p_2 \text{ (when } p_2 < p_3) \text{ or } p_1 < p < p_3 \text{ (when } p_3 < p_2) \tag{B2}$$

(iii) $$\langle\Phi\rangle(p) = \mathcal{H}\Upsilon\left(\kappa\left(\frac{p}{p_2}\right)^3, \kappa\left(\frac{p}{p_1}\right)^3\right) - \left\{2Be^{\kappa}\exp\left[-\kappa\left(\frac{p}{p_2}\right)^3\right] + A\right\} + 2(B + A)e^{\kappa}\exp\left[-\kappa\left(\frac{p}{p_1}\right)^3\right],$$
$$\text{if } p_2 < p_3 \quad \text{and} \quad p_2 < p < p_3 \tag{B3}$$

(iv) $$\langle\Phi\rangle(p) = \mathcal{H}\Upsilon(\kappa, \theta^3\kappa) - B,$$
$$\text{if } p_3 < p_2 \quad \text{and} \quad p_3 < p < p_2 \tag{B4}$$

(v) $$\langle\Phi\rangle(p) = \mathcal{H}\Upsilon\left(\kappa\left(\frac{p}{p_2}\right)^3, \theta^3\kappa\right) - 2Be^{\kappa}\exp\left[-\kappa\left(\frac{p}{p_2}\right)^3\right] + B,$$
$$\text{if } p_3 < p < p_4 \text{ (when } p_2 < p_3) \text{ or } p_2 < p < p_4 \text{ (when } p_3 < p_2) \tag{B5}$$

(vi) $$\langle\Phi\rangle(p) = 0, \quad \text{if } p > p_4, \tag{B6}$$

where

$$p_1 = \frac{\alpha_x D_o}{d_v} + \delta V_o^{1/3}, \tag{B7}$$

$$p_2 = \frac{\beta_x D_o}{d_v} + \delta V_o^{1/3}, \tag{B8}$$

$$p_3 = \theta p_1, \tag{B9}$$

$$p_4 = \theta p_2, \tag{B10}$$

$$\kappa = \frac{\ln 2}{\theta^3 - 1}, \tag{B11}$$

$$\mathcal{K} = 4\gamma_o e^{\kappa} \left(\frac{D_o}{\kappa^{1/3} d_v p} \right)^{\ln 2/\ln \rho}, \tag{B12}$$

and

$$\Upsilon(r, s) = \int_r^s \left[x^{-1/3} - \left(\frac{V_o}{\kappa} \right)^{1/3} \frac{\delta}{p} \right]^{-\ln 2/\ln \rho} \exp(-x)\, dx. \tag{B13}$$

Note that for any given set of parameters and choice of index distribution, either $p_2 < p_3$ or $p_3 < p_2$ so that the forms given by Eqs. (B3) and (B4) are mutually exclusive. $\langle \Phi \rangle (p)$ therefore takes on five distinct functional forms over the range $p > p_R^{max}$: either (i), (ii), (iii), (v), and (vi), when $p_2 < p_3$; or (i), (ii), (iv), (v), and (vi), when $p_3 < p_2$ (see Eqs. B1 to B6).

This work was funded by grants from the Medical Research Council of Canada. Dr. Totafurno gratefully acknowledges the support of an M.R.C. Postdoctoral Fellowship.

Received for publication 16 December 1987 and in final form 16 May 1988.

REFERENCES

Bjerknes, M., and H. Cheng. 1981*a*. The stem cell zone of the small intestinal epithelium. I. Evidence from Paneth cells in the adult mouse. *Am. J. Anat.* 160:51–63.

Bjerknes, M., and H. Cheng. 1981*b*. The stem cell zone of the small intestinal epithelium. IV. Effects of resecting 30% of the small intestine. *Am. J. Anat.* 160:93–103.

Bjerknes, M., and H. Cheng. 1981*c*. A band of alkaline phosphatase activity in the crypts of mouse duodenal epithelium. *J. Histochem. Cytochem.* 29:519–524.

Cairnie, A. B. 1970. Renewal of goblet and Paneth cells in the small intestine. *Cell Tissue Kinet.* 3:35–45.

Cairnie, A. B., and R. E. Bentley. 1967. Cell proliferation studies in the intestinal epithelium of the rat. Hyperplasia during lactation. *Exp. Cell Res.* 46:428–440.

Cairnie, A. B., L. F. Lamerton, and G. G. Steel. 1965*a*. Cell proliferation studies in the intestinal epithelium of the rat. I. Determination of the kinetic parameters. *Exp. Cell Res.* 39:528–538.

Cairnie, A. B., L. F. Lamerton, and G. G. Steel. 1965*b*. Cell proliferation studies in the intestinal epithelium of the rat. II. Theoretical aspects. *Exp. Cell Res.* 39:539–553.

Cheng, H., and M. Bjerknes. 1983. Cell production in mouse intestinal epithelium measured by stathmokinetic flow cytometry and Coulter particle counting. *Anat. Rec.* 207:427–434.

Cheng, H., and C. P. Leblond. 1974. Origin, differentiation, and renewal of the four main epithelial cell types in the mouse small intestine. I. Columnar cell. *Am. J. Anat.* 141:461–480.

Fraser, D. A. S. 1976. Probability and Statistics: Theory and Applications. Duxbury Press, North Scituate, MA.

Kalbfleisch, J. G. 1985. Probability and Statistical Inference. Vol. 1, 2nd edition. Springer-Verlag, New York, Inc.

Lloyd, E. 1984. Handbook of Applicable Mathematics. Vol. VI, Part A. John Wiley & Sons, Toronto.

Mood, A. M., F. A. Graybill, and D. C. Boes. 1974. Introduction to the Theory of Statistics, 3rd edition. McGraw-Hill Book Co., New York.

Pearson, E. S., and H. O. Hartley. 1966. Biometrika Tables for Statisticians. Vol. 1, 3rd edition. Cambridge University Press, Cambridge, England.

Totafurno, J., M. Bjerknes, and H. Cheng. 1987. The crypt cycle: crypt and villus production in the adult intestinal epithelium. *Biophys. J.* 52:279–294.

Wimber, D. R., and L. F. Lamerton. 1963. Cell population studies in the intestine of continuously irradiated rats. *Radiat. Res.* 18:137-146.

Wright, N., and M. Alison. 1984. The Biology of Epithelial Cell Populations. Vol. 2. Clarendon Press, Oxford, England.

Wright, N., A. Morley, and D. R. Appleton. 1972. Variation in the duration of mitosis in the crypts of Lieberkuhn of the rat; a cytokinetic study using vincristine. *Cell Tissue Kinet.* 5:351–364.